Wear-resistant and stable low-friction nanodiamond composite superhard coatings against Al₂O₃ counter-body in dry condition.

DIAB, M.R., MURASAWA, K., IBRAHIM, A.M.M., NARAGINO, H., YOSHITAKE, T. and EGIZA, M.

2025
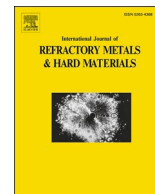
Contents lists available at ScienceDirect

International Journal of Refractory Metals and Hard Materials

Wear-resistant and stable low-friction nanodiamond composite superhard coatings against Al$_2$O$_3$ counter-body in dry condition

Mohamed Ragab Diab [a,b,*], Koki Murasawa [a,c], Ahmed Mohamed Mahmoud Ibrahim [d,e], Hiroshi Naragino [a], Tsuyoshi Yoshitake [a,**], Mohamed Egiza [b,f,*]

[a] *Department of Advanced Energy Science and Engineering, Faculty of Engineering Sciences, Kyushu University, Kasuga, Fukuoka 816-8580, Japan*
[b] *Department of Mechanical Engineering, Kafrelsheikh University, Kafrelsheikh 33516, Egypt*
[c] *OSG Corporation, 3-22 Honnogahara, Toyokawa, Aichi 442-8543, Japan*
[d] *Mechanical and Aerospace Department, College of Engineering, United Arab Emirates University, Al Ain 15551, United Arab Emirates*
[e] *Production Engineering and Mechanical Design department, Faculty of Engineering, Minia University, 61519, Egypt*
[f] *School of Computing, Engineering, and Technology, Robert Gordon University, Aberdeen AB10 7GJ, UK*

ARTICLE INFO

ABSTRACT

Conventional machining lubricants pose environmental hazards and increase production costs. This study addresses this challenge by investigating nanodiamond composite (NDC) coatings deposited on WC–Co substrates as a lubricant-free alternative for sustainable machining. The NDC films show superior hardness (65 GPa) compared to the substrate (22 GPa) and enhanced adhesion (HF2). The NDC's unique self-lubrication results in a low and stable friction coefficient (COF ≤ 0.095) and exceptional wear resistance (7.45×10^{-8} mm^3/N·m) in dry tesing against Al$_2$O$_3$ counter-body. Compared to CVD diamond, NDC coatings show a 47.8 % reduction in COF and a 31.65 % enhancement in wear resistance, promoting environmentally friendly machining practices.

1. Introduction

Machining, a cornerstone of global manufacturing, relies on advances in tool materials to improve efficiency, productivity, and part quality [1]. However, the conventional approach heavily relies on lubricants and coolants, posing significant environmental and health concerns [2]. Cutting fluids, essential for machining critical automotive components such as connecting rods and crankshafts, are major cost drivers and environmental hazards. Studies have linked their usage to both increased production costs (up to 17 %) and worker health issues (80 % of skin diseases) due to exposure to mist and fumes [3]. Stringent environmental regulations and growing worker safety concerns necessitate minimizing or eliminating the use of cutting fluids, with disposal costs often exceeding that of the machining process itself.

This economic and environmental burden has fueled the exploration of sustainable machining alternatives, such as dry machining and minimum quantity lubrication (MQL) [4]. The shift towards sustainable practices empowers companies to improve worker health and safety while simultaneously reducing costs. Sustainable manufacturing prioritizes energy efficiency, environmental protection, waste reduction, and

cost-effective production [5]. Dry machining is considered the most environmentally friendly option, minimizing waste generation and disposal costs altogether [6]. Embracing sustainable machining practices ensures continued high-quality, cost-effective production with minimal environmental impact, safeguarding the well-being of future generations [7].

Sustainable machining of hard-to-cut materials, including carbon fiber-reinforced polymers, Al-Si alloys, ceramics such as alumina (Al$_2$O$_3$), and titanium alloys, presents a distinct challenge [8]. These materials demand specific properties from cutting tools, such as high hardness and toughness, low friction, and excellent wear and corrosion resistance. While Co-cemented tungsten carbide (WC−Co) offers the optimal substrate material for achieving enhanced toughness [9], its wear resistance and hardness are limited due to the Co bonding materials between the WC particles. Therefore, hard-applied coatings are crucial to address these challenges, extending tool life, and improving surface integrity of the final product [10].

During machining, cutting tools experience extreme mechanical forces and temperatures [11], necessitating resistance to friction, wear, corrosion, oxidation, and fatigue [12]. Advanced protective coatings are

---

* Corresponding authors at: Department of Mechanical Engineering, Kafrelsheikh University, Kafrelsheikh 33516, Egypt.
** Corresponding author.
E-mail addresses: mohamed.diab@kyudai.jp (M.R. Diab), Tsuyoshi_yoshitake@kyudai.jp (T. Yoshitake), Mohamed_Egiza@eng.kfs.edu.eg (M. Egiza).

crucial to meet industry demands for increased production efficiency and reduced costs [13]. Notably, these advancements also aim to minimize reliance on hazardous lubricants and coolants [14]. Techniques such as physical and chemical vapor deposition (PVD and CVD) create wear-resistant coatings that enhance tool life and performance. These hard-coated cutting tools remain dominant (85 % of cemented carbide tools are coated) due to their extended tool life and ability to handle advanced materials [15,16]. Additionally, these coatings can be tailored with various materials and designs to suit specific applications [17,18].

Diamond and related hard carbon films, including diamond-like carbon (DLC), are highly desirable for hard coatings on cutting tools [19,20]. However, achieving optimal performance presents a complex challenge. While Chemical Vapor Deposition (CVD) provides a route for diamond coating deposition, it faces limitations in terms of deposition rate, environmental impact, and adhesion of diamond to the commonly used WC−Co substrate [21,22].

CVD processes often involve hazardous chemicals during deposition and pre-treatment, contributing to environmental concerns [23,24]. Additionally, the etching of cobalt atoms from the WC−Co surface, which is crucial for diamond growth, can compromise tool life by weakening the substrate [25,26]. Furthermore, high temperatures and slow deposition rates associated with CVD lead to high energy consumption and increased production costs [27]. Moreover, the resulting diamond coatings often exhibit high surface roughness, impacting tribological performance [28]. While hot filament CVD (HF-CVD) allows for thick diamond coatings, their performance is hindered by the catalytic effects of cobalt, leading to diamond graphitization and weakened adhesion [29]. DLC, particularly ta-C films, offers advantages such as lower friction and simpler deposition processes. However, their inherent limitations include high internal stress, thinness, and consequently, frequent tool changes, impacting cost-effectiveness [30]. To address these shortcomings and promote sustainable machining practices, nanodiamond composite (NDC) films have emerged as a promising solution. These films feature a unique nanostructure with embedded nanodiamond crystals within an amorphous carbon (a-C) matrix. This innovative design has the potential to combine the exceptional hardness and wear resistance of diamond with the smooth surface, cost-effectiveness, and potentially lower environmental impact of DLC coatings, making them a viable option for sustainable machining applications.

Coaxial arc plasma deposition (CAPD) is a particularly attractive method for depositing NDC films due to its sustainability benefits compared to traditional CVD [31]. CAPD eliminates the need for external substrate heating, harsh chemical reactions during deposition, and the environmentally hazardous process of etching cobalt atoms from the WC−Co substrate [32–34]. Additionally, CAPD boasts higher deposition rates, minimizing production time and energy consumption. Furthermore, CAPD offers superior control over film properties [35,36]. Compared to CVD, CAPD allows for precise tailoring of the NDC film's morphology and thickness for specific applications. Notably, CAPD-produced films exhibit a high sp^3 content [37,38], indicating a more diamond-like structure, and lower internal stress (around 4.5 GPa) compared to ta-C films. This combination has the potential to enhance wear resistance and achieve a desirable film thickness without delamination challenges.

High-performance cutting tools require a delicate balance between exceptional wear resistance and low friction to minimize energy consumption and heat generation during machining. Understanding the interplay between these properties at the nanoscale is crucial, especially since cutting tools operate under dynamic contact conditions [39]. Material characteristics such as crystalline structure, hardness, elasticity, and surface roughness all influence the tribological properties of materials, which encompass both friction and wear.

This work aims to investigate the viability of NDC coatings as a sustainable alternative for cutting tools. The primary objective is to develop NDC coatings with exceptional wear resistance achieved through a combination of high hardness, substantial thickness, and a smooth surface. To accomplish this, NDC films will be deposited on WC−Co substrates and subjected to a systematic analysis of their characteristics. This analysis will include a direct comparison with conventional CVD diamond films deposited on the same substrates to objectively evaluate the performance of NDC coatings. The deposited NDC films will be assessed for morphology, structure, mechanical properties (hardness, Young's modulus, adhesion), and tribological behavior (coefficient of friction, wear mechanisms). This comprehensive approach evaluates the suitability of NDC coatings for sustainable machining applications by comparing their performance to the existing standard.

2. Experimental procedures

2.1. Films synthesis

NDC and CVD diamond coatings were deposited on WC−Co substrates ($\varphi 10 \times 5.5$ mm, K-type cemented tungsten carbide with 6 wt% Co) using distinct techniques tailored to each coating material. Diamond films were deposited using the Hot Filament Chemical Vapor Deposition (HF-CVD) method at a temperature of approximately 800 °C, with a deposition rate of 0.5 μm per hour. Before coating, the WC−Co substrates were prepared through a two-step etching process: first, surface roughening was achieved with Murakami's reagent, producing a surface roughness (Ra) of 0.15–0.2 μm; this was followed by cobalt removal using an acidic hydrogen peroxide solution. Finally, nanodiamond seeding was performed in an ultrasonic bath, an essential step for promoting diamond growth [13].

NDC films were synthesized on unheated WC−Co substrates using a CAPD technique with a high-purity graphite target (99.9 %), achieving a higher deposition rate of 3.5 μm/h. This process employed an arc plasma gun (ULVAC, APG-1000) under specific conditions (120 V, 1 Hz repetition rate, 720 μF capacitor), resulting in thicker films (10 μm), comparable to those produced by CVD diamond. The CAPD chamber was maintained at a low pressure (less than 10^{-4} Pa) using a turbomolecular pump, without the introduction of chemical gases. To enhance adhesion, the WC−Co substrates only underwent a roughening treatment (Ra ≈ 0.15–0.2 μm) prior to NDC deposition. For tribological wear testing, pin-shaped WC−Co samples (20 mm length, 6 mm diameter) were prepared with various coated spherical ends, making them suitable for pin-on-disk friction and wear tests.

2.2. Films characterization

The hardness and Young's modulus of the coatings were measured by nanoindentation. This involved multiple tests at randomly selected 20 points per sample using a Berkovich diamond indenter (Fisher Instruments, HM500). Film adhesion was evaluated separately using a Rockwell diamond indenter at the same load (150 kg), featuring an apex angle of 120° and a radius of the top ending sphere of 0.2 mm.

Friction and wear resistance were investigated through pin-on-disk friction tests. In these tests, the coated WC−Co pins (NDC and CVD diamond) were rubbed against polished alumina (Al_2O_3) disks (3 mm thick, 20 mm diameter) without lubrication in the open air at room temperature (around 25 °C) and relative constant humidity. The tests were conducted at a linear speed of 20 cm/s, with a normal load of 300 g, and at varying durations (10, 30, and 60 min) to assess wear behavior. Wear resistance was quantified by measuring the worn volume, area, and depth of the coatings on the pin samples using a 3D laser confocal microscope (Olympus LEXT OLS5000, Japan).

To understand the morphology of the deposited films, top-view images were acquired using field emission scanning electron microscopy (FE-SEM, JEOL/JSM-IT700HR). Additionally, Raman spectroscopy was used to characterize the structural properties of the coatings. This

analysis was also performed on the CVD diamond coatings for comparison. Raman spectra were collected using a Lambda Vision Raman spectroscopic system (MicroRAM-300ATG) equipped with a confocal microscope and a high-performance detector. The samples were illuminated with a 532 nm laser beam, and the acquired spectra were analyzed to identify the various bonding configurations within the coatings.

3. Results and discussion

3.1. Sustainable films growth and structural analysis

The study successfully achieved the deposition of NDC films on WC−Co substrates with a high deposition rate (3.5 μm/h), significantly exceeding that of CVD diamond films (7 times faster). This translates to significant time and cost savings during the deposition process. Furthermore, NDC films maintained structural integrity at a thickness of 10 μm, comparable to CVD diamond coatings. This increased thickness of NDC films has the potential to improve their wear resistance in cutting applications. Another key advantage of the NDC deposition process lies in its sustainability. Unlike CVD diamond processes requiring external substrate heating (800 °C), NDC films were deposited without external substrate heating, leading to significant energy savings. Additionally, the CAPD method eliminates the need for chemical etching of cobalt atoms from the substrate, a hazardous step associated with traditional pre-treatment processes. The deposition of NDC films aligns well with sustainability goals by promoting energy efficiency, cost-effectiveness, and environmentally friendly practices.

Fig. 1 presents the distinct surface morphologies of the as-deposited CVD diamond and NDC coatings revealed by FE-SEM. The CVD diamond film (Fig. 1a) exhibits a rougher surface texture with numerous well-defined micro-sized diamond grains (1–3 μm) exhibiting pyramidal shapes and orientations. These observations are consistent with the high average roughness (Ra) value of 195 nm measured for the CVD diamond film (Fig. 2a).

In contrast, the NDC film (Fig. 1b) displays a denser structure with a "cauliflower" morphology characterized by rounded domes of relatively uniform size. This indicates homogeneous growth on the WC−Co substrate and fine clustering. The observed columnar growth and high film thickness (10 μm) can be attributed to the film's structure influenced by the highly energetic carbon species (C$^+$) ejected from the CAPD anode [40] and the inherent surface roughness of the WC−Co substrate. Notably, this thickness allows NDC films to potentially address a wider range of cutting applications.

The surface roughness of the coatings, as measured by the average roughness (Ra) parameter, further supports the observations from FE-SEM analysis (Fig. 1). The CVD diamond film exhibits higher Ra value (195 nm), reflecting its rougher surface texture caused by the presence of faceted diamond grains (Fig. 2a). Conversely, the NDC film displays a smoother topography with a lower Ra value (159 nm), attributed to its "cauliflower-type" morphology (Fig. 2b). Interestingly, both the CVD diamond and NDC films retain a significant influence from the initial roughness of the WC−Co substrate (Ra = 150–200 nm).

Finally, Fig. 2c presents the topography of the counterpart material used in the tribological evaluation, an alumina (Al$_2$O$_3$) disk with a rough surface texture (Ra = 355 nm, Sa = 427 nm). This challenging surface reflects the abrasive nature of the material to be cut during machining operations.

3.1.1. Raman analysis

Raman spectroscopy provided valuable insights into the structural characteristics of the deposited films, particularly the sp^2 and sp^3 carbon
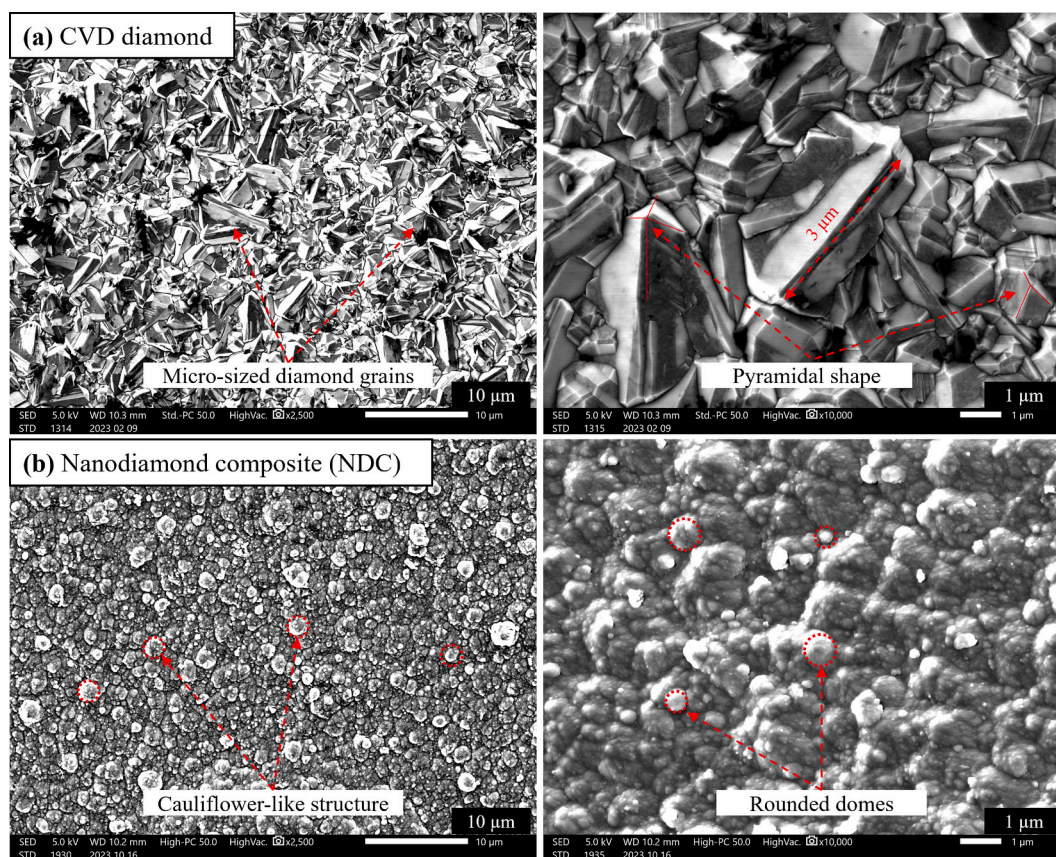

Fig. 1. Top-view FE-SEM images of as-deposited CVD diamond and NDC coatings.(For interpretation of the references to color in this figure legend, the reader is referred to the web version of this article.)
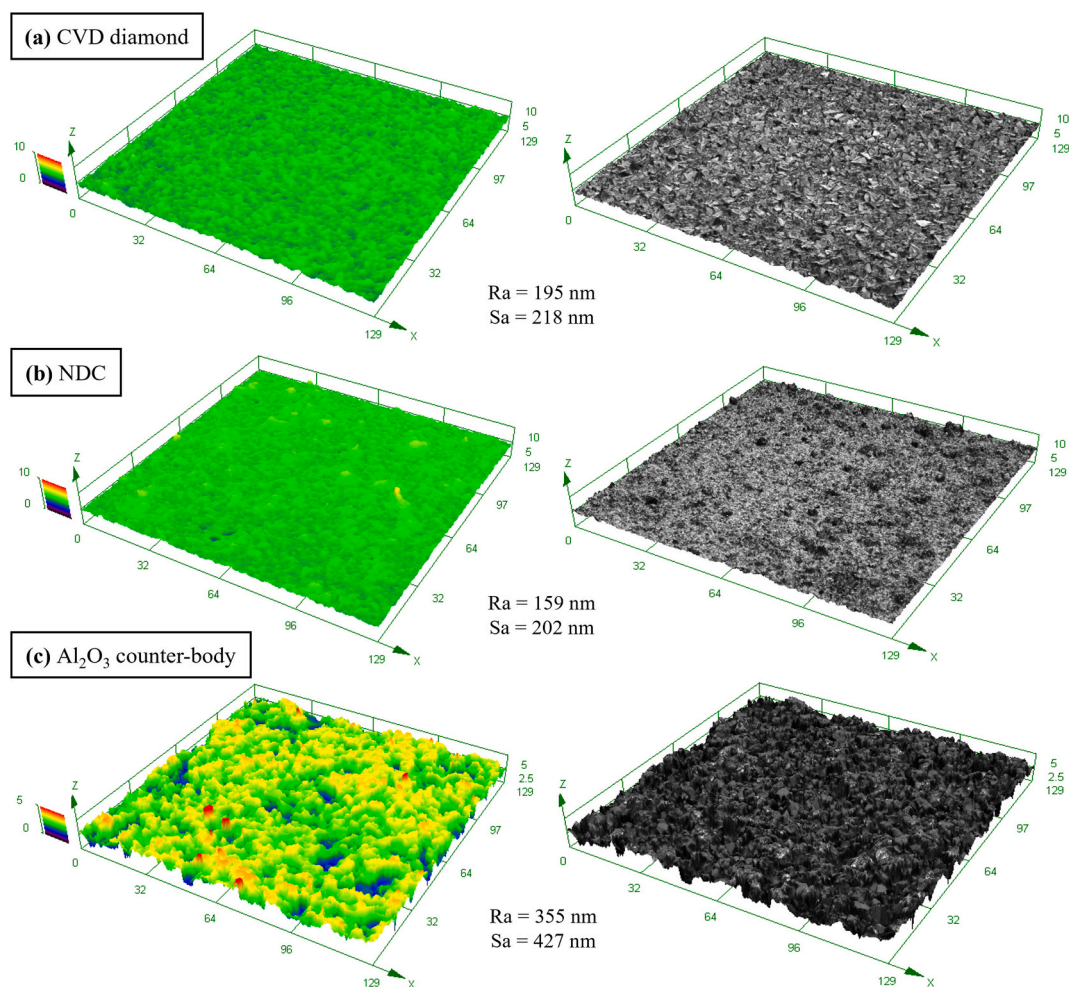
Fig. 2. Surface topographies of (a) CVD diamond film, (b) NDC film, and (c) Al_2O_3 disk, accompanied by their respective measured surface roughness values. (For interpretation of the references to color in this figure legend, the reader is referred to the web version of this article.)
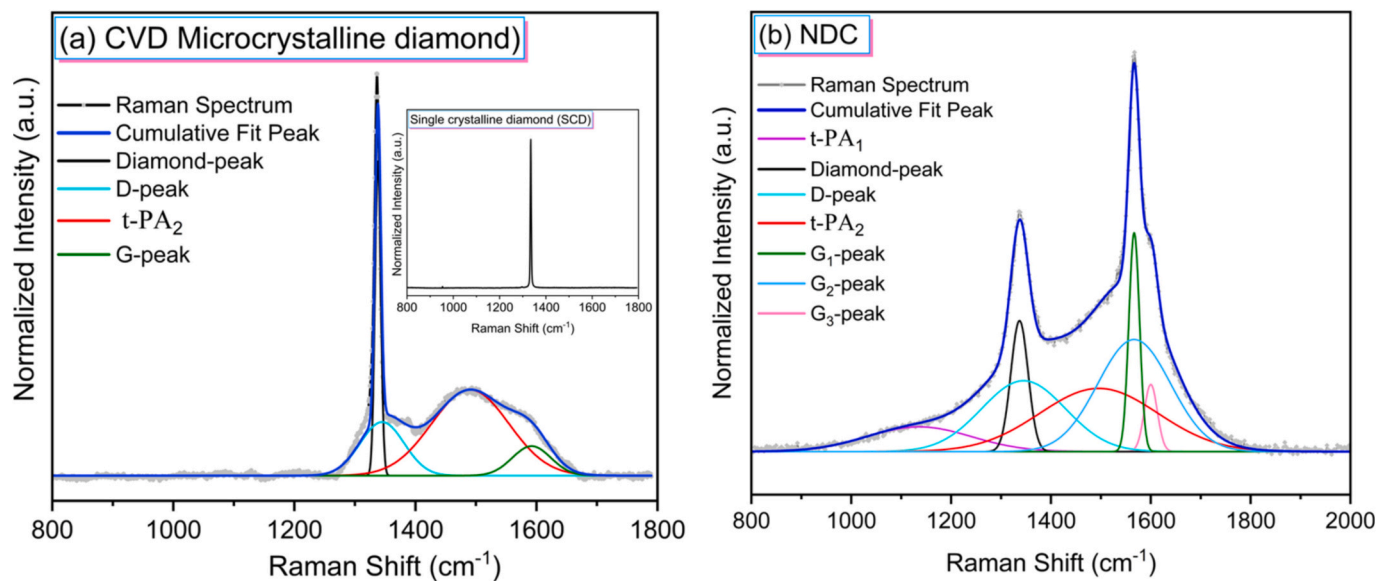

Fig. 3. Decomposed Raman spectra of (a) CVD diamond and (b) NDC films along with the spectrum of single crystal diamond (SCD) for comparison (onset). (For interpretation of the references to color in this figure legend, the reader is referred to the web version of this article.)

phases. To obtain detailed information, the collected visible Raman spectra of CVD diamond and NDC films were deconvoluted into individual component peaks using a Gaussian function (Fig. 3). This deconvolution revealed distinct features including *trans*-polyacetylene (t-PA) peaks, the diamond peak, D-peak, and G-peak.

The presence of t-PA peaks, corresponding to sp^2-hybridized carbon segments primarily located at grain boundaries within the films, sheds light on the microstructure [41,42]. These segments consist of carbon atoms bonded alternately with a hydrogen atom and another carbon atom (C=C—C—H). Previous studies have shown a strong correlation between t-PA peaks and the abundance of grain boundaries in nanocomposite films [41,43]. Notably, the NDC films exhibited t-PA peaks, with t-PA$_1$ at 1140 cm^{-1} and t-PA$_2$ at 1496 cm^{-1}. Interestingly, an increase in the intensity of one t-PA peak often coincides with a decrease in the other, as observed in CVD diamond films where the t-PA$_2$ peak increased significantly while the t-PA$_1$ peak diminished. These observations suggest the presence of a high number of grain boundaries within the NDC films, attributed to the small nanodiamond grain size. These grain boundaries play a crucial role in relieving compressive stress within the film, ultimately facilitating the growth of thicker NDC films, and achieving thicknesses comparable to CVD diamond.

A single crystal diamond (SCD) reference sample was used to calibrate the Raman spectrometer, confirming the characteristic first-order Raman diamond peak for C—C sp^3 bonding at 1332 cm^{-1}. However, slight shifts in the diamond peak position for the deposited films were observed. These shifts can be attributed to factors such as laser heating, defects, film structure disorder, and impurities [44]. The observed broadening and slight shift towards higher wavenumbers in the diamond peak of the deposited films can be explained by two key factors: reduced phonon confinement length due to the nanodiamond characteristics and internal stress within the films [45,46]. Compressive stress typically shifts the peak towards higher wavenumbers, while tensile stress shifts it towards lower wavenumbers. This relationship can be described by Eq. (1):

$$\sigma = -0.567 \, (\nu - \nu_o) \tag{1}$$

where σ represents internal stress (GPa), ν is the measured diamond peak wavenumber (cm^{-1}), ν_o is the reference wavenumber of stress-free diamond (1332 cm^{-1}), and K is a material constant [47].

The CVD diamond film exhibited a diamond peak at 1338 cm^{-1}, indicating a compressive internal stress of approximately 3.4 GPa. In contrast, the NDC film displayed a diamond peak at 1337 cm^{-1}, suggesting a lower compressive stress of about 2.835 GPa. This observation aligns with the presence of grain boundaries due to the nanodiamond phase formation within the NDC films, which likely contributes to the suppression of internal stress compared to CVD diamond and most hard DLC films (typically experiencing 5–16 GPa of stress) [48,49].

The Raman spectra revealed a D-peak at 1345 cm^{-1} in the NDC film, similar to CVD diamond and ta-C films. This peak typically observed between 1300 cm^{-1} and 1380 cm^{-1} in various carbon forms, signifies the presence of disordered or defective sp^2 carbon structures with dangling bonds within the amorphous matrix of the films [50]. Notably, in the NDC and CVD diamond films, the D-peak coincides with the diamond peak in the visible Raman spectra, suggesting the existence of amorphous or graphitic carbon at grain boundaries [51]. These grain boundaries in NDC films are thought to impede dislocation movement, potentially leading to increased mechanical strength, as supported by Rockwell testing results.

The G-peak typically appears between 1510 cm^{-1} and 1580 cm^{-1} but can extend to 1600 cm^{-1} with a high presence of sp^3 carbon chains [52,53]. This peak originates from the in-plane stretching vibration of carbon atoms in the hexagonal lattice structure, encompassing both ring and chain configurations [41]. Shifts in the G-peak position are influenced by bond disorder and sp^3 chain formation. Lower wavenumbers indicate higher disorder, while higher wavenumbers suggest greater sp^3

chain formation [54].

The asymmetric G-peak profile in the NDC films, with three components centered at 1566 cm^{-1} (G$_1$ & G$_2$) and 1600 cm^{-1} (G$_3$), stands in contrast to the symmetric G-peaks observed in CVD diamond (1591 cm^{-1}) and ta-C films (1545 cm^{-1}). This difference suggests a more complex interplay between sp^2 and sp^3 hybridization within the NDC films. The presence of the G$_3$-peak at a higher wavenumber (1600 cm^{-1}) aligns with the potential conversion of sp^2 carbon rings to sp^3 carbon chains, as previously discussed. This conversion might facilitate the formation of small carbon clusters, as observed in SEM images. These sp^3 chains within the NDC film matrix likely contribute to its enhanced hardness.

The hardness of NDC films appears to originate from a combination of factors revealed by Raman spectroscopy. The presence of nanodiamond grains within the amorphous carbon matrix, along with features such as ring and chain graphite phases observed through the G-peak analysis, collectively influence the hardness of the NDC films. The grain boundaries, as suggested by the t-PA peaks, may also contribute to enhanced mechanical strength by impeding dislocation movement.

3.2. Mechanical properties of NDC films

3.2.1. Hardness and adhesion assessment

Nanoindentation measurements demonstrated a remarkable hardness of 65 GPa for the NDC coatings compared with 22 GPa of the WC−Co substrate, and 80 GPa for the CVD diamond film. This significant enhancement in hardness directly translates into a potential improvement in the wear resistance of WC−Co cutting tools, making them more durable during machining operations.

However, achieving strong adhesion between these coatings and the WC−Co substrate remains a challenge, as evidenced by Rockwell indentation tests (Fig. 4). While etching techniques have been employed to mitigate detrimental Co catalytic effects at the interface, delamination has occurred for CVD diamond specimens, particularly at higher testing loads [55]. This highlights the limitations of their basic deposition processes without incorporating additional methods to enhance film adhesion, such as buffer layers, thermal annealing, or doping with foreign elements [21,26].

The NDC films exhibited superior adhesion strength compared to CVD diamond, which aligns with the residual stress measurements obtained through Raman spectroscopy. Higher residual compressive stress is known to decrease adhesion strength. Consequently, the NDC coating deposited at room temperature by the CAPD technique exhibits the strongest coating-substrate interface due to its lower residual stress and suppressed Co-catalytic effects at the interface.

A key advantage of the CAPD technique lies in its ability to address the challenge of Co diffusion [56], a major hurdle encountered in traditional CVD methods for depositing diamond films on substrates containing iron (Fe), cobalt (Co), or nickel (Ni) [29]. During CAPD, high-energy carbon ions (C$^+$) bombard the substrate interface [40,57], promoting the formation of a dense NDC film (Fig. 5). This dense structure effectively hinders Co diffusion into the film, thereby preventing detrimental graphitization, as confirmed by the weakened EDS Co spectrum, particularly at the interface. The dense NDC film itself is characterized by a high concentration of strong sp^3-bonded carbon atoms, resembling the structure of amorphous diamond [58]. This dense film structure effectively suppresses Co diffusion while maintaining a significant sp^3 bonding content within the film itself.

3.3. Tribological properties

3.3.1. Coefficient of friction

The tribological performance of the deposited hard carbon coatings (CVD diamond and NDC films) was evaluated using a pin-on-disk tribometer under dry conditions at room temperature (Fig. 6). This investigation aimed to assess the feasibility of using NDC films for sustainable
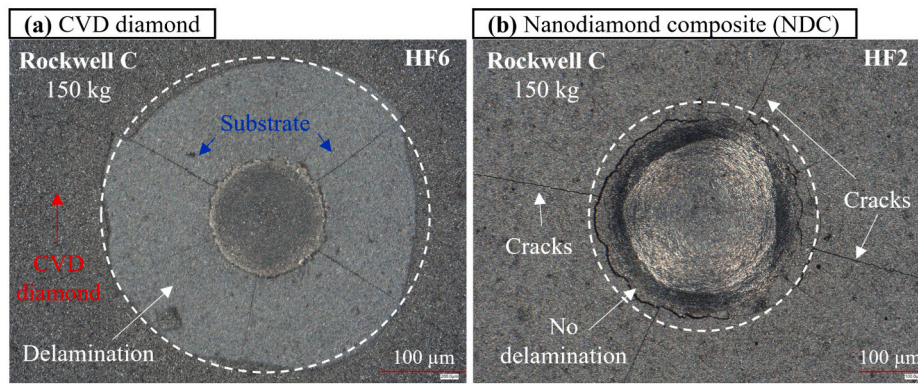
Fig. 4. Optical microscopic images after Rockwell C toughness testing for (a) CVD diamond and (b) NDC coatings. (For interpretation of the references to color in this figure legend, the reader is referred to the web version of this article.)
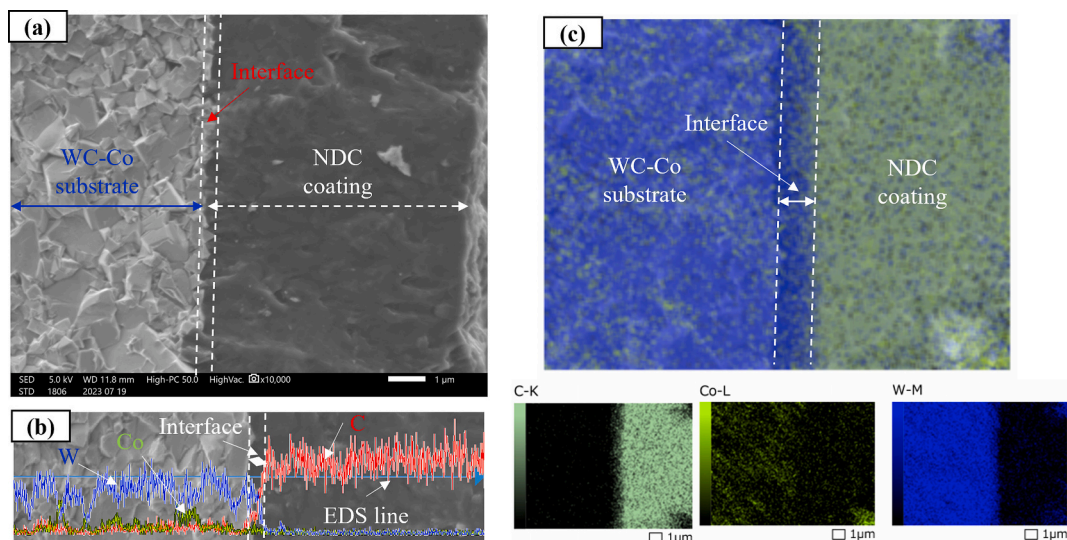

Fig. 5. Cross-sectional SEM image, (b) corresponding EDS spectra, and (c) EDS mapping of the NDC film. (For interpretation of the references to color in this figure legend, the reader is referred to the web version of this article.)
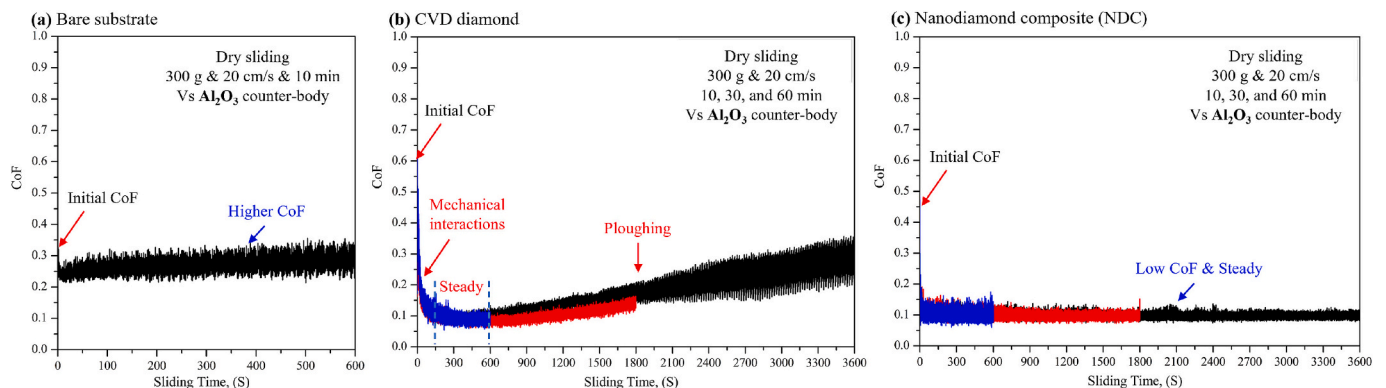

Fig. 6. Coefficient of friction for (a) bare substrate, (b) CVD diamond, and (c) NDC films vs. Al$_2$O$_3$ counter-body. (For interpretation of the references to color in this figure legend, the reader is referred to the web version of this article.)

machining of difficult-to-cutmaterials, such as the notoriously hard and abrasive Al$_2$O$_3$. The coefficient of friction (COF) was continuously monitored throughout the tests at various sliding periods, followed by an evaluation of wear resistance.

Friction and wear performance of carbon-based coatings are influenced by a complex interplay of intrinsic and extrinsic factors [59]. Intrinsic factors include the degree of sp^3 bonding within the film and the specific balance between sp^2 and sp^3 hybridization on the film's surface. These intrinsic properties significantly affect the tribological characteristics. Extrinsic factors encompass the test environment and

tribological conditions, such as contact pressure, sliding speed, and ambient temperature [60].

Surface roughness is another critical factor influencing friction and wear. Rougher surfaces experience increased mechanical interlocking between asperities, leading to higher friction, particularly during the initial stages of sliding (Fig. 7). This highlights the importance of considering both intrinsic film properties and extrinsic test conditions when evaluating tribological performance for specific applications.

CVD diamond films exhibited a three-stage wear evolution (Fig. 6, Fig. 7) influenced by interactions between surface features, modifications during sliding, and wear debris generation. The initial stage is characterized by a rapidly changing and high friction coefficient due to mechanical interactions between asperities on the diamond film and the rough Al_2O_3 counter-body. Ploughing by these asperities creates abrasive wear, with furrows and debris formation. Shearing forces also fracture diamond grains referring to the weak adhesion between the diamond grains and the substrate, adding to the abrasive particles in the contact zone. As the asperities wear away and the initial surface interactions stabilize, the friction coefficient reaches a more consistent value.

Stage II features a significantly lower and more stable friction coefficient. This reduction is primarily due to a decrease in adhesion between the film and the counter body caused by the formation of a graphite-rich tribo layer film on the diamond surface. This tribofilm facilitates the sliding of the rubbing surfaces and contributes to the low wear volume observed during this stage.

After 600 s of sliding time, the wear process transitions to Stage III. This stage is marked by a rapid rise in the friction coefficient due to the generation and accumulation of wear debris acting as third-body particles within the contact zone. These wear debris, mainly composed of hard diamond debris, cause significant ploughing friction and accelerated wear of the coating. The wear track morphology exhibits localized areas of spallation and cracks within the remaining diamond film. The initial loose wear debris likely agglomerates into larger particles over time. This accumulation, combined with additional debris from delamination, surpasses a critical threshold by the end of Stage II. Consequently, Stage III is dominated by the ploughing action of these large, hard-wear particles, leading to a severe abrasive wear regime. The increasing friction coefficient due to the growing presence of third-body particles, combined with higher shear stresses, further accelerates the wear and eventual breakdown of the CVD diamond coating.

NDC films exhibited a similar three-stage wear behavior with distinct characteristics (Fig. 6, Fig. 7). The initial running-in stage features a high friction peak due to wear debris generation (NDC and Al_2O_3 fragments). This is followed by a transition process and a steady-state stage with a very low and stable COF (0.095). The low friction coefficient is attributed to the self-lubricating properties of NDC films, their unique nanostructure comprises the presence of nanodiamond crystals embedded within an amorphous carbon matrix. Additionally, the high hardness and moderate surface roughness of NDC films contribute to their superior tribological performance compared to CVD diamond films.

3.3.2. Wear mechanism

Examination of the worn surfaces by FE-SEM revealed that abrasive wear was the dominant wear mechanism during the tribological tests (Fig. 8, Fig. 9). This conclusion aligns with the challenging test conditions, which employed a highly abrasive Al_2O_3 counter-body under dry sliding conditions.

Abrasive wear occurs when hard asperities on the Al_2O_3 disk concentrate pressure and break down the asperities of the CVD diamond film upon contact. This breakdown process produces wear debris particles from both the film and the counter-body (Al_2O_3). These wear debris particles then act as cutting wedges, creating deep grooves on the diamond surface. These particles can be either loosely distributed or become adhered to the contacting surfaces. The high contact pressures experienced during the tests can exacerbate abrasive wear by inducing severe plastic deformation of the debris particles, contributing significantly to the abrasive wear of the CVD diamond films.

Adhesive wear, characterized by material transfer between contacting surfaces, played a minimal role in this experiment. While real surfaces exhibit roughness leading to localized contact points, the observed lack of significant material transfer suggests minimal adhesion between the diamond film and the Al_2O_3 counter body. Nevertheless, plastic deformation at these contact points can create work-hardened regions exceeding the strength of the underlying diamond material. The subsequent fracture of these micro-protrusions can lead to the generation of wear debris. These particles can then contribute to the ongoing wear process by acting as additional abrasive elements within the contact zone.

Abrasive wear has also been identified as the primary wear mechanism for NDC films (Fig. 8, Fig. 9). However, the exceptional tribological performance of NDC coatings, characterized by stabilized low friction and high wear resistance, arises from a combination of factors beyond its inherent hardness.

The unique nanostructure of NDC films, consisting of nanodiamond grains embedded within an amorphous carbon (a-C) matrix [40], contributes to their wear resistance. This combination provides an ultra-
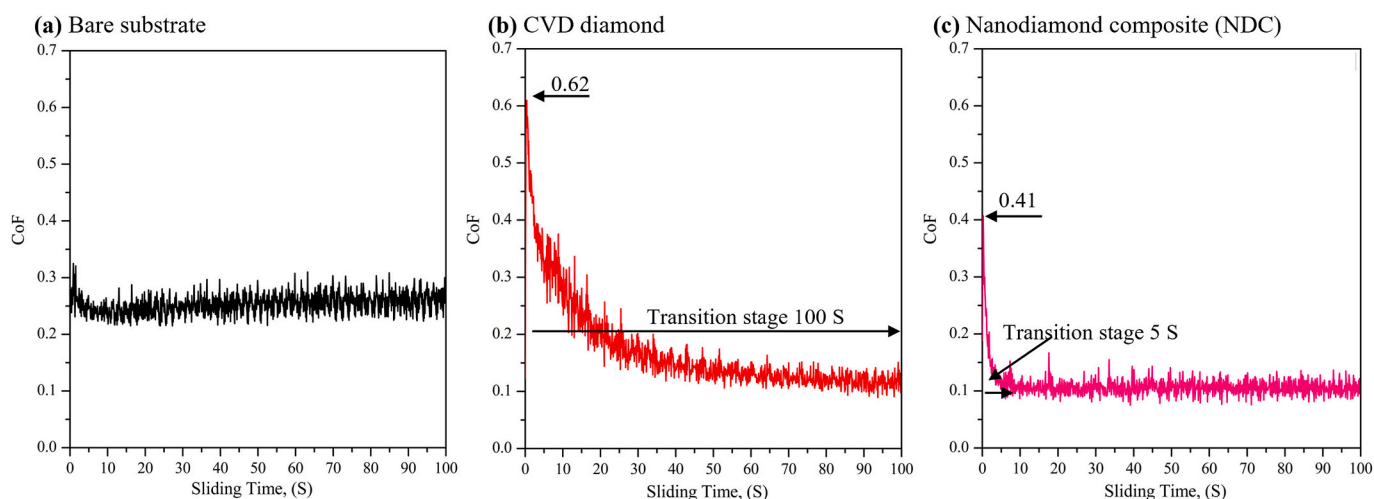

Fig. 7. Comparison between initial COF and transition stage for (a) bare substrate, (b) CVD diamond, and (c) NDC films vs. Al_2O_3 counter-body. (For interpretation of the references to color in this figure legend, the reader is referred to the web version of this article.)
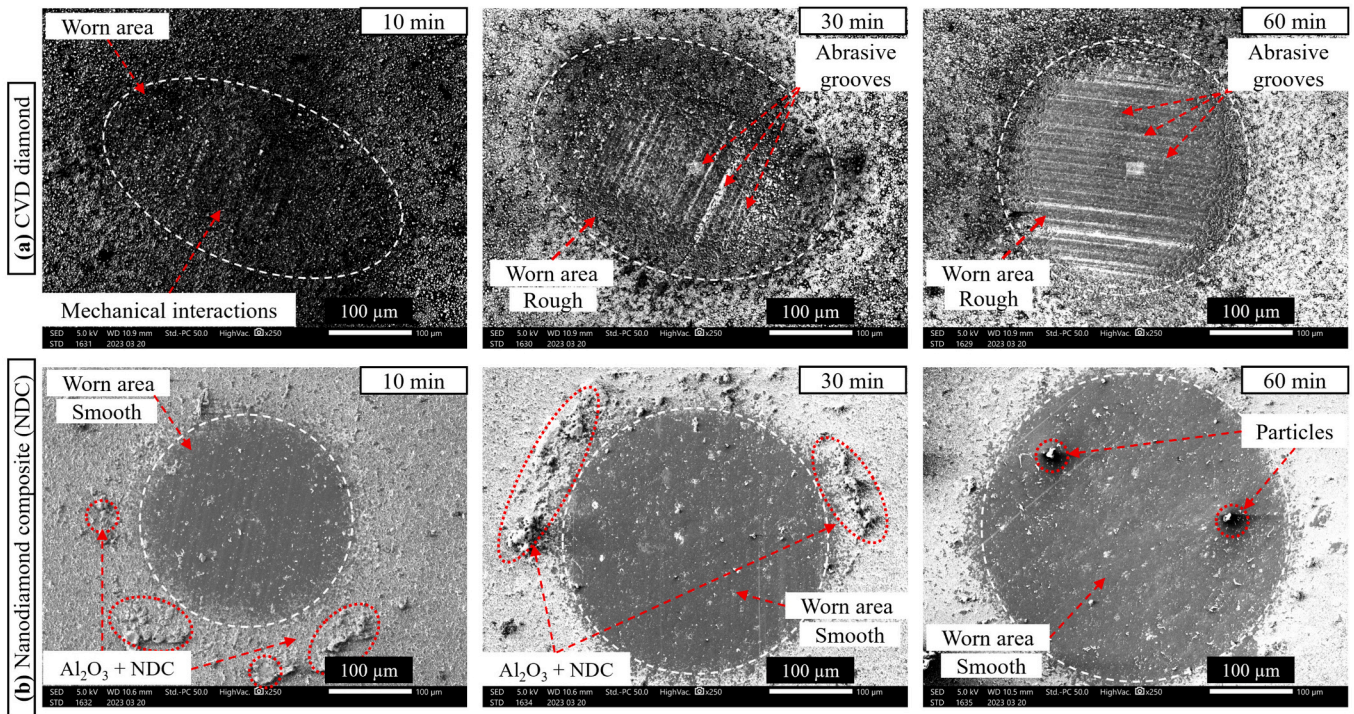
Fig. 8. Wear appearance of pin samples after friction test at various periods of 10, 30, and 60 min: (a) CVD diamond and (b) NDC coatings. (For interpretation of the references to color in this figure legend, the reader is referred to the web version of this article.)

Fig. 9. Wear appearance of Al_2O_3 counter-body tracks after friction test at various periods of 10, 30, and 60 min: (a) CVD diamond and (b) NDC coatings. (For interpretation of the references to color in this figure legend, the reader is referred to the web version of this article.)
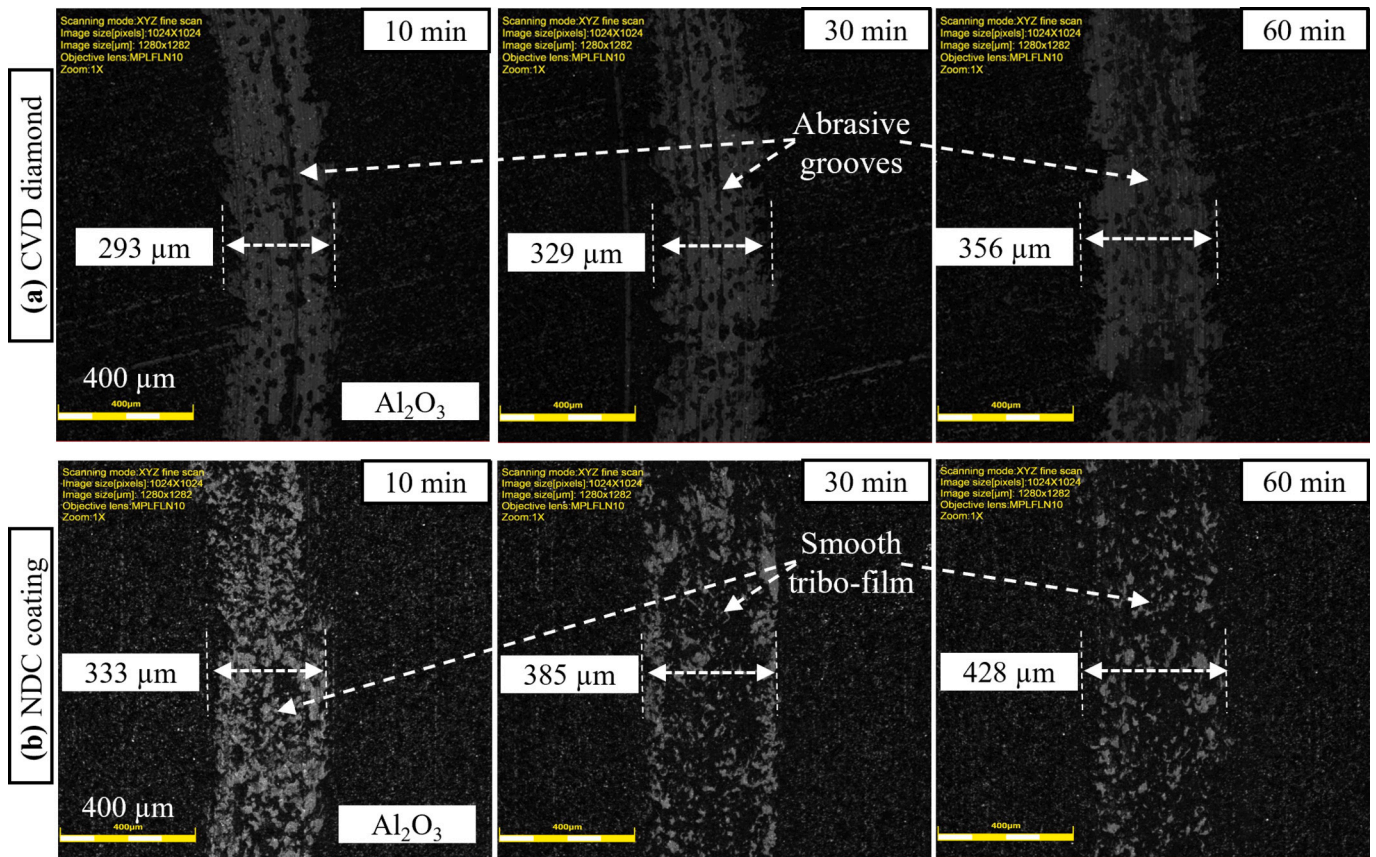
smooth surface with exceptional mechanical properties, including high hardness (65 GPa) and Young's modulus (688 GPa). During the sliding process, plastic deformations within the a-C matrix can potentially lead to a gradual strengthening of the near-surface region, forming a protective shell that resists wear. However, the formation of a tribo-layer during sliding contact plays a crucial role in achieving the ultra-low friction and wear characteristics of NDC films. Recent studies emphasize the importance of both surface chemistry and the tribological environment in determining these behaviors.

Surface passivation and chemical rehybridization from sp^3 to sp^2 bonding are key factors influencing the tribological performance of NDC films. This rehybridization process involves the transformation of the sp^3 phase of carbon into the sp^2 phase, leading to the formation of graphite or amorphous carbon [61]. These rehybridized phases act as solid lubricants, effectively reducing the coefficient of friction by minimizing direct contact between the sliding surfaces.

The presence of both nanodiamond grains and the a-C phase within the tribe-film plays a synergistic role in achieving significant reductions in friction and wear [39]. The a-C matrix facilitates the formation of this lubricating layer, minimizing direct contact and reducing friction and wear.

3.3.3. Quantifying wear resistance

Wear resistance [62,63], a critical performance metric in tribology, is typically evaluated by measuring several parameters of the worn surfaces: wear volume, worn area, wear depth, and the wear track width on the Al$_2$O$_3$ counter body (Fig. 10, Fig. 11). These evaluations were conducted using a 3D laser confocal microscope. The wear rate of the films was calculated using the Archard Eq. (2) [64]:

$$k = \frac{V}{F \times L} \tag{2}$$

where k denotes the wear rate (mm^3/N·m), V denotes the wear volume (mm^3), F denotes the normal load (N), and L denotes the total sliding distance (m).

Fig. 10 presents a comparative analysis of wear depth for CVD diamond and NDC coatings after sliding against alumina (Al$_2$O$_3$) counter-body for varying durations (10, 30, and 60 min). This figure highlights the superior wear resistance of NDC coatings across all tested sliding times. Fig. 11 further strengthens this observation by illustrating

the average COF and wear rates for both coatings alongside the bare WC−Co substrate. The substrate achieved COF value of 0.3 and wear resistance of 1.28×10^{-6} mm^3/N·m after 10 min.

CVD diamond exhibits a concerning trend of increasing COF values (from 0.112 to 0.182) and wear resistance (from 1.07×10^{-7} mm^3/N·m to 8.41×10^{-8} mm^3/N·m) with extended sliding times. This phenomenon can be attributed to ploughing effects, where the harder CVD diamond asperities (microscopic protrusions) plow through the softer Al$_2$O$_3$ counter-body, leading to increased material removal and friction.

Conversely, the COF of NDC coatings demonstrates a slightly decreasing trend (from 0.103 to 0.095) with increasing sliding time. This behavior is consistent with the self-lubricating mechanism observed in Fig. 8, where the surface droplets and amorphous carbon matrix potentially create a lubricating tribo-film during sliding contact. This tribo-film could reduce friction by minimizing direct asperity contact between the coating and the counter-body. Crucially, the wear rate of NDC coatings remains significantly lower resulting in higher wear resistance (1.09×10^{-7} mm^3/N·m to 7.45×10^{-8} mm^3/N·m) compared to CVD diamond throughout the experiment.

The reduction in COF from CVD to NDC is approximately 47.8 %. Additionally, the enhancement in wear resistance from CVD to NDC is approximately 31.65 %. These findings underscore the potential advantages of NDC coatings over CVD diamond in applications demanding high wear resistance and low friction. The significant reduction in wear rate signifies the enhanced wear resistance of NDC coatings, making them a potentially superior choice for cutting tool applications.

3.4. Sustainable and comparative performance assessment of NDC and CVD diamond coatings

Manufacturing is shifting towards eco-friendly technologies that extend cutting tool life and optimize surface parameters while minimizing costs. Dry machining, which eliminates cutting fluids, represents a sustainable approach, enhancing machinability and reducing environmental toxicity. This technique can lower production costs by 16–20 % while effective coating configurations can further reduce tool wear and friction [65].

3.4.1. Economic and environmental analysis

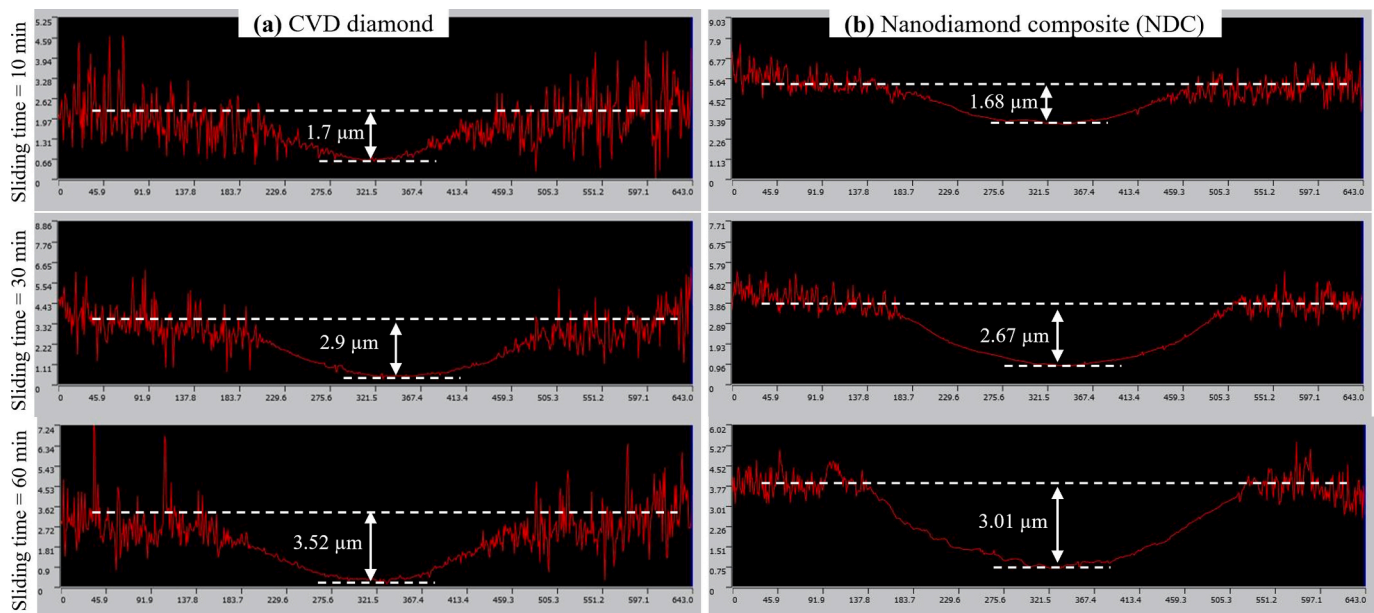The CAPD technique, utilized for the synthesis of NDC coatings,

Fig. 10. Depth profiles after friction wear test of (a) CVD diamond and (b) NDC films at various durations of 10, 30, and 60 min. (For interpretation of the references to color in this figure legend, the reader is referred to the web version of this article.)

Fig. 11. Wear evaluation for CVD diamond and NDC films on Al$_2$O$_3$ at 300 g and 200 mm/s for 10, 30, and 60 min. (For interpretation of the references to color in this figure legend, the reader is referred to the web version of this article.)
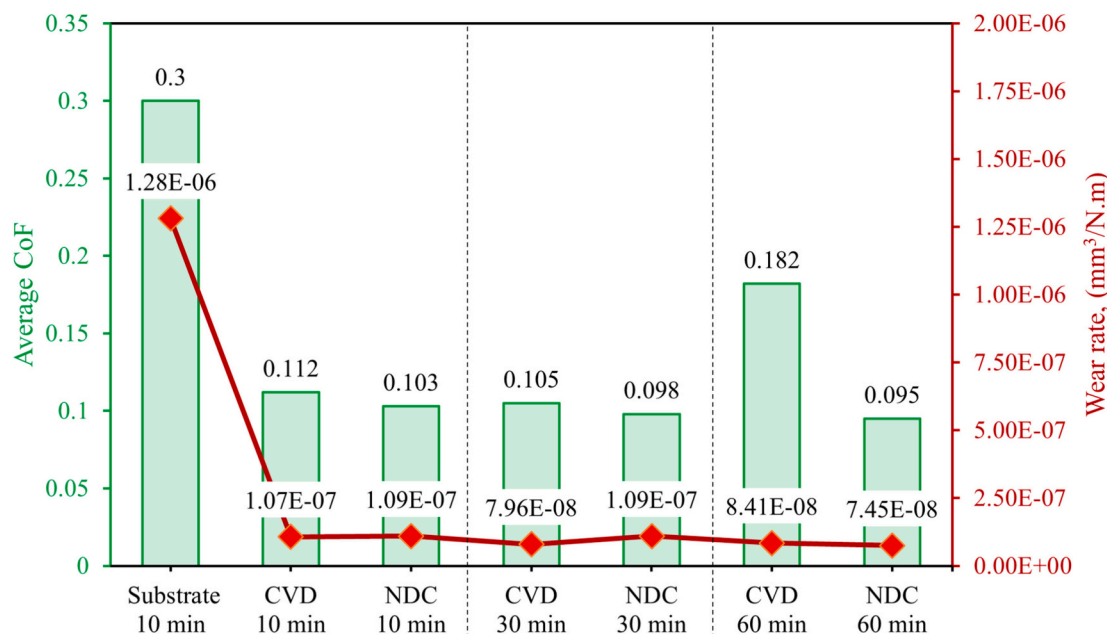
offers significant economic advantages compared to conventional CVD methods. The CAPD system features a simplified architecture that includes a vacuum setup with mechanical and turbomolecular pumps, a 304-grade stainless-steel deposition chamber, an arc gun, and monitoring viewports. In contrast, CVD systems are characterized by more complex configurations that incorporate microwave or hot filament plasma sources. Additionally, CAPD employs a closed-loop water chiller to cool the turbomolecular pump, whereas CVD systems require additional cooling measures for the deposition chamber, leading to higher costs and stricter operational safety regulations.

The safety profile of CAPD further enhances its economic viability. The process eliminates the need for hazardous gases and utilizes a straightforward operational protocol. CAPD's reliance on a pure graphite target rod is more cost-effective than the expensive gases and specialized flow systems mandated in CVD processes. Moreover, the deposition rate of the CAPD technique (3.5 μm/h) significantly exceeds that of the CVD method (0.5 μm/h), resulting in reduced production time and lower overall costs. This reduction in material costs also diminishes ongoing safety expenditures associated with the handling and disposal of toxic materials. Moreover, the elimination of external heaters and reactive gases contributes to lower operational costs.

From an environmental standpoint, traditional CVD techniques have a considerable ecological footprint. These processes typically consume large volumes of chemical gases and hazardous substances, such as sodium hydroxide and water, resulting in substantial material waste. Additionally, the need for etching cobalt from the substrate surface in CVD processes consumes hazardous chemicals and adds costs associated with diamond-coated tools. Conversely, NDC coatings are deposited on WC−Co substrates in a vacuum environment, thus eliminating the need for harsh chemicals and toxic gases typically used in substrate pretreatment and CVD diamond synthesis. This reduction in environmental pollutants not only enhances workplace safety but also protects the surrounding ecosystem and the health of workers.

3.4.2. Energy consumption analysis

Energy consumption is a critical factor in the production of high-performance coatings, with conventional methods often proving to be energy-intensive. The CAPD technique, however, offers notable energy efficiency. In the CAPD framework, the cathodic arc gun serves as the

primary energy consumer, accounting for approximately 82 % of total energy usage, which equates to around 65 kWh per deposition cycle. In contrast, auxiliary components such as pumps, heating, etching, and cooling contribute a minor fraction, collectively consuming about 11.6 kWh.

The total energy consumption in the production of NDC coatings can be estimated using the following formula (3):

$$\text{Total energy consumption} = \left(E_{discharge} \times t_{deposition}\right) + E_{others} \tag{3}$$

where $E_{discharge}$ is the coating energy consumption (KW), $t_{deposition}$ is deposition time (h), and E_{others} is other components like pumps, heating, etching, and cooling (kWh).

When compared to the CVD method, CAPD exhibits remarkable energy efficiency, with total energy consumption values of 974 kWh for CVD and only 53.5 kWh for CAPD [66]. Additionally, CAPD significantly reduces process cycle times, achieving comparable results within a 3-h cycle, in contrast to the 18.5 h required for CVD.

The efficiency of CAPD is further highlighted by the thickness of the coatings produced. Both CVD and CAPD yield coatings of 10 μm;

Table 1

Comparison between NDC coatings fabricated by eco-friendly CAPD and well-established CVD diamond coatings fabricated by HF-CVD.

Case study	NDC coatings	CVD diamond coatings
Fabrication technique	CAPD	HF-CVD
Substrate	Cemented carbide (WC−6 %Co)	
Pre-treatment	Roughening	Roughening + etching of Co + seeding
Coating sources	Pure graphite target	Hydrogen (H$_2$) and methane (CH$_4$)
Deposition time, (hr)	3	20
Deposition temperature, (°C)	Room temperature	800
Deposition rate, (μm/h)	3.5	0.5
Layer thickness, (μm)	10	10
Compressive stress, (GPa)	2.835	3.4
Hardness, (GPa)	65	80
Adhesion	HF2	HF6
CoF (Dry against Al$_2$O$_3$)	0.095 (Stable)	0.182 (Unstable)
Wear rate, (mm^3/N.m)	7.45×10^{-8}	8.41×10^{-8}

however, CAPD accomplishes this with a substantially lower energy requirement of 6.5 kWh/μm, whereas CVD necessitates 97.4 kWh/μm.

3.4.3. Comparative performance assessment

Table 1 provides a detailed comparison of NDC coatings and CVD diamond coatings, emphasizing the distinct mechanical and tribological advantages offered by NDC coatings, particularly in the context of sustainable manufacturing. NDC coatings, synthesized using the eco-friendly CAPD technique, present several key benefits that enhance their viability as alternatives to those produced via HF-CVD.

A significant advantage of NDC coatings is their deposition process, which occurs at room temperature. This characteristic enhances substrate compatibility and minimizes energy consumption compared to the high temperatures (approximately 800 °C) required for CVD coatings. Additionally, NDC coatings achieve a markedly higher deposition rate of 3.5 μm/h, compared to the 0.5 μm/h rate of CVD coatings. This increased efficiency results in faster production cycles and lower operational costs.

Mechanical performance metrics further underscore the competitiveness of NDC coatings. While CVD coatings exhibit superior hardness at 80 GPa and compressive stress of 3.4 GPa, NDC coatings maintain commendable hardness levels of 65 GPa with lower compressive stress (2.8 GPa), which enhances adhesion strength. Notably, NDC coatings demonstrate better adhesion (HF2) than CVD coatings (HF6), improving their reliability in cutting tool applications.

Tribological assessments reveal that NDC coatings exhibit a lower coefficient of friction (0.095) compared to CVD coatings (0.182), indicating enhanced stability and efficiency in dry machining conditions. Furthermore, NDC coatings exhibit a reduced wear rate of 7.45×10^{-8} mm^3/N·m compared to CVD coatings (8.41×10^{-8} mm^3/N·m), highlighting their superior wear resistance and longevity in cutting applications.

4. Conclusion

This study investigated the potential of nanodiamond composite (NDC) coatings deposited using the environmentally friendly coaxial arc plasma deposition (CAPD) technique for sustainable machining applications. NDC coatings were compared to conventional hot filament CVD diamond coatings deposited on WC−Co substrates. The investigation revealed several key advantages of NDC films. First, the CAPD process successfully deposited thick (10 μm) single-layer NDC films on unheated WC−Co substrates at a rapid deposition rate (3.5 μm/h). Second, these films exhibited superior adhesion properties (HF2) compared to CVD diamond films (HF6). Importantly, NDC films exhibited exceptional tribological performance. Despite a slightly rougher surface resulting in a higher initial COF, they maintained a remarkably stable and low COF (0.095) even against a challenging Al$_2$O$_3$ counter-body under dry conditions for extended testing durations (60 min). This superior performance is attributed to the combined effect of the film's high hardness, Young's modulus, toughness, and the presence of grain boundaries and an amorphous carbon matrix, promoting a self-lubricating effect. Finally, NDC films showcased excellent wear resistance (7.45×10^{-8} mm^3/N·m), further highlighting their potential for sustainable machining applications. These findings strongly suggest that NDC films are a promising alternative to traditional CVD diamond coatings. Their superior adhesion, wear resistance, and ability to maintain low friction under harsh conditions make them strong contenders for advancing cutting tool technology and related industrial applications.

CRediT authorship contribution statement

Mohamed Ragab Diab: Writing – original draft, Validation, Methodology, Formal analysis. **Koki Murasawa:** Validation, Resources, Methodology. **Ahmed Mohamed Mahmoud Ibrahim:** Writing – review & editing, Validation, Methodology. **Hiroshi Naragino:** Visualization,

Resources, Methodology, Investigation. **Tsuyoshi Yoshitake:** Writing – review & editing, Supervision, Funding acquisition. **Mohamed Egiza:** Writing – review & editing, Writing – original draft, Project administration.

Declaration of competing interest

The authors declare that they have no known competing financial interests or personal relationships that could have appeared to influence the work reported in this paper.

Data availability

Data will be made available on request.

References

[1] I.S. Jawahir, J. Schoop, Y. Kaynak, A.K. Balaji, R. Ghosh, T. Lu, Progress toward modeling and optimization of sustainable machining processes, J. Manuf. Sci. Eng. (2020) 142, https://doi.org/10.1115/1.4047926.
[2] S. Qin, Z. Li, G. Guo, Q. An, M. Chen, W. Ming, Analysis of minimum quantity lubrication (MQL) for different coating tools during turning of TC11 titanium alloy, Materials (2016) 9, https://doi.org/10.3390/ma9100804.
[3] K. Ishfaq, I. Anjum, C.I. Pruncu, M. Amjad, M.S. Kumar, M.A. Maqsood, Progressing towards sustainable machining of steels: a detailed review, Materials (2021) 14, https://doi.org/10.3390/ma14185162.
[4] F. Klocke, G. Eisenblätter, Dry cutting, CIRP Ann. 46 (1997) 519–526, https://doi.org/10.1016/S0007-8506(07)60877-4.
[5] K. Gupta, R.F. Laubscher, Sustainable machining of titanium alloys: a critical review, Proc. Inst. Mech. Eng. B J. Eng. Manuf. 231 (2016) 2543–2560, https://doi.org/10.1177/0954405416634278.
[6] G.S. Goindi, P. Sarkar, Dry machining: a step towards sustainable machining – challenges and future directions, J. Clean. Prod. 165 (2017) 1557–1571, https://doi.org/10.1016/j.jclepro.2017.07.235.
[7] N. Khanna, J. Wadhwa, A. Pitroda, P. Shah, J. Schoop, M. Sarıkaya, Life cycle assessment of environmentally friendly initiatives for sustainable machining: a short review of current knowledge and a case study, Sustain. Mater. Technol. 32 (2022) e00413, https://doi.org/10.1016/j.susmat.2022.e00413.
[8] N. Geier, J.P. Davim, T. Szalay, Advanced cutting tools and technologies for drilling carbon fibre reinforced polymer (CFRP) composites: a review, Compos. A: Appl. Sci. Manuf. 125 (2019) 105552, https://doi.org/10.1016/j.compositesa.2019.105552.
[9] A. Bicherl, T. Zimmerl, G. Mühlbauer, S. Geroldinger, A. Bock, When tungsten meets carbon, Int. J. Refract. Met. Hard Mater. 119 (2024) 106448, https://doi.org/10.1016/j.ijrmhm.2023.106448.
[10] K. Yamamoto, M. Abdoos, P. Stolf, B. Beake, S. Rawal, G. Fox-Rabinovich, et al., Cutting performance of low stress thick TiAlN PVD coatings during machining of compacted graphite cast Iron (CGI), Coatings 8 (2018) 38, https://doi.org/10.3390/coatings8010038.
[11] A. Inspektor, P.A. Salvador, Architecture of PVD coatings for metalcutting applications: a review, Surf. Coat. Technol. 257 (2014) 138–153, https://doi.org/10.1016/j.surfcoat.2014.08.068.
[12] N. Schalk, M. Tkadletz, C. Mitterer, Hard coatings for cutting applications: physical vs. chemical vapor deposition and future challenges for the coatings community, Surf. Coat. Technol. 429 (2022) 127949, https://doi.org/10.1016/j.surfcoat.2021.127949.
[13] Z. Yuan, Y. Guo, C. Li, L. Liu, B. Yang, H. Song, et al., New multilayered diamond/β-SiC composite architectures for high-performance hard coating, Mater. Des. 186 (2020) 108207, https://doi.org/10.1016/j.matdes.2019.108207.
[14] A.H. Abdelrazek, I.A. Choudhury, Y. Nukman, S.N. Kazi, Metal cutting lubricants and cutting tools: a review on the performance improvement and sustainability assessment, Int. J. Adv. Manuf. Technol. 106 (2020) 4221–4245, https://doi.org/10.1007/s00170-019-04890-w.
[15] A. Baptista, F. Silva, J. Porteiro, J. Míguez, G. Pinto, Sputtering physical vapour deposition (PVD) coatings: a critical review on process improvement and market trend demands, Coatings 8 (2018) 402, https://doi.org/10.3390/coatings8110402.
[16] F. Lofaj, M. Kabátová, L. Kvetková, J. Dobrovodský, V. Girman, Hybrid PVD-PECVD W-C:H coatings prepared by different sputtering techniques: The

comparison of deposition processes, composition and properties, Surf. Coat. Technol. 375 (2019) 839–853, https://doi.org/10.1016/j.surfcoat.2019.07.078.

[17] X. Liu, H. Zhang, G. Lin, Z. Wang, J. Zhang, H. Shi, Advances in deposition of diamond films on cemented carbide and progress of diamond coated cutting tools, Vacuum 217 (2023) 112562, https://doi.org/10.1016/j.vacuum.2023.112562.

[18] G. Madhavi, N. Kishan, C.R. Raghavendra, A review on recent approaches in the field of surface coating, Mater. Today: Proc. 52 (2022) 403–406, https://doi.org/10.1016/j.matpr.2021.09.075.

[19] Y. Zhao, F. Xu, D. Zhang, J. Xu, X. Shi, S. Sun, et al., Enhanced tribological and corrosion properties of DLC/CrN multilayer films deposited by HPPMS, Ceram. Int. 48 (2022) 25569–25577, https://doi.org/10.1016/j.ceramint.2022.05.236.

[20] K. Murasawa, M.R. Diab, M. Wang, H. Naragino, T. Yoshitake, M. Egiza, Influence of droplet-free ta-C coatings and lubrication conditions on tribological performance and mechanical characteristics of WC–Co, Mater. Lett. (2024) 372, https://doi.org/10.1016/j.matlet.2024.137058.

[21] M. Lu, H. Wang, X. Song, F. Sun, Effect of doping level on residual stress, coating-substrate adhesion and wear resistance of boron-doped diamond coated tools, J. Manuf. Process. 88 (2023) 145–156, https://doi.org/10.1016/j.jmapro.2023.01.041.

[22] R. Dumpala, N. Kumar, C.R. Kumaran, S. Dash, B. Ramamoorthy, M. S. Ramachandra Rao, Adhesion characteristics of nano- and micro-crystalline diamond coatings: Raman stress mapping of the scratch tracks, Diam. Relat. Mater. 44 (2014) 71–77, https://doi.org/10.1016/j.diamond.2014.02.007.

[23] R. Polini, Chemically vapour deposited diamond coatings on cemented tungsten carbides: substrate pretreatments, adhesion and cutting performance, Thin Solid Films 515 (2006) 4–13, https://doi.org/10.1016/j.tsf.2005.12.042.

[24] Y.S. Li, A. Hirose, The effects of substrate compositions on adhesion of diamond films deposited on Fe-base alloys, Surf. Coat. Technol. 202 (2007) 280–287, https://doi.org/10.1016/j.surfcoat.2007.05.037.

[25] B. Sahoo, A.K. Chattopadhyay, On effectiveness of various surface treatments on adhesion of HF-CVD diamond coating to tungsten carbide inserts, Diam. Relat. Mater. 11 (2002) 1660–1669, https://doi.org/10.1016/s0925-9635(02)00137-1.

[26] F. Ye, Y. Li, X. Sun, Q. Yang, C.-Y. Kim, A.G. Odeshi, CVD diamond coating on WC-Co substrate with Al-based interlayer, Surf. Coat. Technol. 308 (2016) 121–127, https://doi.org/10.1016/j.surfcoat.2016.06.088.

[27] Y.S. Li, Y. Tang, Q. Yang, C. Xiao, A. Hirose, Growth and adhesion failure of diamond thin films deposited on stainless steel with ultra-thin dual metal interlayers, Appl. Surf. Sci. 256 (2010) 7653–7657, https://doi.org/10.1016/j.apsusc.2010.06.022.

[28] R. Polini, M. Barletta, On the use of CrN/Cr and CrN interlayers in hot filament chemical vapour deposition (HF-CVD) of diamond films onto WC-Co substrates, Diam. Relat. Mater. 17 (2008) 325–335, https://doi.org/10.1016/j.diamond.2007.12.059.

[29] X.J. Li, L.L. He, Y.S. Li, Q. Yang, Catalytic graphite mechanism during CVD diamond film on iron and cobalt alloys in CH4-H2 atmospheres, Surf. Coat. Technol. 360 (2019) 20–28, https://doi.org/10.1016/j.surfcoat.2018.12.120.

[30] Y.B. Zhang, S.P. Lau, D. Sheeja, B.K. Tay, Study of mechanical properties and stress of tetrahedral amorphous carbon films prepared by pulse biasing, Surf. Coat. Technol. 195 (2005) 338–343, https://doi.org/10.1016/j.surfcoat.2004.09.009.

[31] M. Egiza, M. Ragab Diab, A.M. Ali, K. Murasawa, T. Yoshitake, Sustainable super-hard and thick nanodiamond composite film deposited on cemented carbide substrates with an interfacial Al-interlayer, Mater. Lett. (2024) 364, https://doi.org/10.1016/j.matlet.2024.136369.

[32] M.R. Diab, M. Egiza, K. Murasawa, S. Ohmagari, H. Naragino, T. Yoshitake, Revealing mechanical and structural properties of Si-doped nanodiamond composite films through applied biasing voltages on WC − Co substrates, Int. J. Refract. Met. Hard Mater. (2024) 119, https://doi.org/10.1016/j.ijrmhm.2023.106518.

[33] M. Egiza, A.M. Ali, K. Murasawa, T. Yoshitake, B-doped nanodiamond composite hard coatings deposited on cemented carbide: mechanical, structural, and tribological properties, Int. J. Refract. Met. Mater. (2023) 114, https://doi.org/10.1016/j.ijrmhm.2023.106260.

[34] M. Egiza, A.M. Ali, M.R. Diab, N. Hemaya, K. Murasawa, T. Yoshitake, Synthesis and comprehensive synchrotron-based structural analysis of Si-doped nanodiamond composite films deposited on cemented carbide, Surf. Coat. Technol. (2023) 471, https://doi.org/10.1016/j.surfcoat.2023.129867.

[35] M. Egiza, M. Ragab Diab, H. Atta, M.M. Abdelfatah, A. El-Shaer, T. Yoshitake, Unveiling a 72.5 GPa peak hardness in sustainable nanodiamond composite hard coatings via discharge energy control: a nanoindentation-Raman approach, Mater. Lett. (2024) 369, https://doi.org/10.1016/j.matlet.2024.136684.

[36] M. Egiza, M.R. Diab, K. Murasawa, H. Naragino, T. Yoshitake, Nanomechanical and structural characteristics of nanodiamond composite films dependent on target-substrate distance, Arab. J. Sci. Eng. (2024), https://doi.org/10.1007/s13369-024-09161-9.

[37] M. Egiza, H. Naragino, A. Tominaga, K. Hanada, K. Kamitani, T. Sugiyama, et al., Effects of air exposure on hard and soft X-ray photoemission spectra of Ultrananocrystalline diamond/amorphous carbon composite films, Coatings (2018) 8, https://doi.org/10.3390/coatings8100359.

[38] M. Egiza, H. Naragino, A. Tominaga, K. Murasawa, H. Gonda, M. Sakurai, et al., Si and Cr doping effects on growth and mechanical properties of UltrananocrystallineDiamond/amorphous carbon composite films deposited on cemented carbide substrates by coaxial arc plasma deposition, Evergreen 3 (2016) 32–36, https://doi.org/10.5109/1657738.

[39] R. Rani, K.J. Sankaran, K. Panda, N. Kumar, K. Ganesan, S. Chakravarty, et al., Tribofilm formation in ultrananocrystalline diamond film, Diam. Relat. Mater. 78 (2017) 12–23, https://doi.org/10.1016/j.diamond.2017.07.009.

[40] H. Naragino, A. Tominaga, K. Hanada, T. Yoshitake, Synthesis method for ultrananocrystalline diamond in powder employing a coaxial arc plasma gun, Appl. Phys. Express (2015) 8, https://doi.org/10.7567/apex.8.075101.

[41] A.C. Ferrari, J. Robertson, Origin of the1150 cm^{-1} Raman mode in nanocrystalline diamond, Phys. Rev. B 63 (2001), https://doi.org/10.1103/PhysRevB.63.121405, 121405(R).

[42] M.R. Diab, M. Egiza, K. Murasawa, H. Naragino, A. El-Shaer, T. Yoshitake, Eco-friendly thick and wear-resistant nanodiamond composite hard coatings deposited on WC–Co substrates, Surf. Coat. Technol. (2024) 479, https://doi.org/10.1016/j.surfcoat.2024.130517.

[43] B. Paramanik, D. Das, Synthesis of nanocrystalline diamond embedded diamond-like carbon films on untreated glass substrates at low temperature using (C2H2 + H2) gas composition in microwave plasma CVD, Appl. Surf. Sci. (2022) 579, https://doi.org/10.1016/j.apsusc.2021.152132.

[44] L. Zhang, H. Li, K.-T. Yue, S.-L. Zhang, X. Wu, J. Zi, et al., Effects of intense laser irradiation on Raman intensity features of carbon nanotubes, Phys. Rev. B (2002) 65, https://doi.org/10.1103/PhysRevB.65.073401.

[45] A. Roy, D. Das, Synthesis of single-walled, bamboo-shaped and Y-junction carbon nanotubes using microwave plasma CVD on low-temperature and chemically processed catalysts, J. Phys. Chem. Solids (2021) 152, https://doi.org/10.1016/j.jpcs.2021.109971.

[46] X. Song, M. Lu, H. Wang, X.C. Wang, F.H. Sun, Fracture mechanics of microcrystalline/nanocrystalline composited multilayer chemical vapor deposition self-standing diamond films, Ceram. Int. 48 (2022) 21868–21878, https://doi.org/10.1016/j.ceramint.2022.04.173.

[47] C.T. Kuo, C.R. Lin, H.M. Lien, Origins of the residual stress in CVD diamond films, Thin Solid Films 290-291 (1996) 254–259, https://doi.org/10.1016/s0040-6090(96)09016-5.

[48] J.-K. Shin, C.S. Lee, K.-R. Lee, K.Y. Eun, Effect of residual stress on the Raman-spectrum analysis of tetrahedral amorphous carbon films, Appl. Phys. Lett. 78 (2001) 631–633, https://doi.org/10.1063/1.1343840.

[49] Y. Yin, D.R. McKenzie, J. Zou, A. Das, The application of the cathodic arc to plasma assisted chemical vapor deposition of carbon, J. Appl. Phys. 79 (1996) 1563–1568, https://doi.org/10.1063/1.362649.

[50] H.-j. Wang, D.-w. Zuo, F. Xu, W.-z. Lu, Fabrication of Nano-crystalline diamond duplex Micro-gear by hot filament chemical vapor deposition, Mater. Trans. 58 (2017) 91–94, https://doi.org/10.2320/matertrans.M2016334.

[51] A. Dychalska, P. Popielarski, W. Franków, K. Fabisiak, K. Paprocki, M. Szybowicz, Study of CVD diamond layers with amorphous carbon admixture by Raman scattering spectroscopy, Mater. Sci.-Pol. 33 (2015) 799–805, https://doi.org/10.1515/msp-2015-0067.

[52] A.C. Ferrari, J. Robertson, Raman spectroscopy of amorphous, nanostructured, diamond–like carbon, and nanodiamond, Philos. Trans. R. Soc. London, Ser. A 362 (2004) 2477–2512, https://doi.org/10.1098/rsta.2004.1452.

[53] K. Aoki, K. Suzuki, K. Ishii, K. Takanashi, T. Komukai, K. Oura, et al., Formation of nanoscale diamond particles without substrate heating by cathodic arc deposition, Jpn. J. Appl. Phys. (2005) 44, https://doi.org/10.1143/jjap.44.L746.

[54] A.C. Ferrari, A.C. Ferrari, J. Robertson, Raman spectroscopy of amorphous, nanostructured, diamond–like carbon, and nanodiamond, Philos. Trans. R. Soc. London, Ser. A 362 (2004) 2477–2512, https://doi.org/10.1098/rsta.2004.1452.

[55] G. Straffelini, P. Scardi, A. Molinari, R. Polini, Characterization and sliding behavior of HFCVD diamond coatings on WC–Co, Wear 249 (2001) 461–472, https://doi.org/10.1016/s0043-1648(01)00574-9.

[56] K. Murasawa, M.R. Diab, H. Atta, H. Naragino, A. El-Shaer, T. Yoshitake, et al., Disclosing mechanical and specific structural characteristics of thick and adherent nanodiamond composite hard coating deposited on WC−Co substrates, Mater. Today Commun. (2024) 40, https://doi.org/10.1016/j.mtcomm.2024.109839.

[57] A.M. Ali, T. Deckert-Gaudig, M. Egiza, V. Deckert, T. Yoshitake, Near- and far-field Raman spectroscopic studies of nanodiamond composite films deposited by coaxial arc plasma, Appl. Phys. Lett. 116 (2020) 5, https://doi.org/10.1063/1.5142198.

[58] M.A. Caro, V.L. Deringer, J. Koskinen, T. Laurila, G. Csányi, Growth mechanism and origin of high sp3 content in tetrahedral amorphous carbon, Phys. Rev. Lett. 120 (2018) 166101, https://doi.org/10.1103/PhysRevLett.120.166101.

[59] O.L. Eryilmaz, J.A. Johnson, O.O. Ajayi, A. Erdemir, Deposition, characterization, and tribological applications of near-frictionless carbon films on glass and ceramic substrates, J. Phys. Condens. Matter 18 (2006) S1751–S1762, https://doi.org/10.1088/0953-8984/18/32/s06.

[60] E. Ali, D. Christophe, Tribology of diamond-like carbon films: recent progress and future prospects, J. Phys. D. Appl. Phys. 39 (2006) R311, https://doi.org/10.1088/0022-3727/39/18/R01.

[61] A. Gaydaychuk, S. Linnik, Tribological and mechanical properties of diamond films synthesized with high methane concentration, Int. J. Refract. Met. Hard Mater. 85 (2019) 105057, https://doi.org/10.1016/j.ijrmhm.2019.105057.

[62] D. Boing, A.J. de Oliveira, R.B. Schroeter, Evaluation of wear mechanisms of PVD and CVD coatings deposited on cemented carbide substrates applied to hard turning, Int. J. Adv. Manuf. Technol. 106 (2020) 5441–5451, https://doi.org/10.1007/s00170-020-05000-x.

[63] A. Chatterjee, S. Jayaraman, J.E. Gerbi, N. Kumar, J.R. Abelson, P. Bellon, et al., Tribological behavior of hafnium diboride thin films, Surf. Coat. Technol. 201 (2006) 4317–4322, https://doi.org/10.1016/j.surfcoat.2006.08.086.

[64] M. Egiza, M.R. Diab, A.W. Zia, K. Murasawa, N. Faisal, T. Yoshitake, Wear-resistant and adherent nanodiamond composite thin film for durable and sustainable silicon

carbide mechanical seals, Wear 550-551 (2024) 205394, https://doi.org/10.1016/j.wear.2024.205394.

[65] F. Koné, C. Czarnota, B. Haddag, M. Nouari, Modeling of velocity-dependent chip flow angle and experimental analysis when machining 304L austenitic stainless steel with groove coated-carbide tools, J. Mater. Process. Technol. 213 (2013) 1166–1178, https://doi.org/10.1016/j.jmatprotec.2013.01.015.

[66] M. Gassner, M. Rebelo de Figueiredo, N. Schalk, R. Franz, C. Weiß, H. Rudigier, et al., Energy consumption and material fluxes in hard coating deposition processes, Surf. Coat. Technol. 299 (2016) 49–55, https://doi.org/10.1016/j.surfcoat.2016.04.062.